JCTC Journal of Chemical Theory and Computation

Article

pubs.acs.org/JCTC

Asymmetric-Lanczos-Chain-Driven Implementation of Electronic Resonance Convergent Coupled-Cluster Linear Response Theory

Sonia Coriani,*[,†,§] Thomas Fransson,[‡] Ove Christiansen,[§] and Patrick Norman[‡]

[†]Dipartimento di Scienze Chimiche e Farmaceutiche, Università degli Studi di Trieste, I-34127 Trieste, Italy

[‡]Department of Physics, Chemistry and Biology, Linköping University, SE-581 83 Linköping, Sweden

[§]Department of Chemistry, Aarhus University, DK-8000, Århus C, Denmark

ABSTRACT: We present an implementation of the damped coupled-cluster linear response function based on an asymmetric Lanczos chain algorithm for the hierarchy of coupled-cluster approximations CCS (coupled-cluster singles), CC2 (coupled-cluster singles and approximate doubles), and CCSD (coupled-cluster singles and doubles). Triple corrections to the excitation energies can be included via the CCSDR(3) (coupled-cluster singles and doubles with noniterative-triples-corrected excitation energies) approximation. The performance and some of the potentialities of the approach are investigated in calculations of the visible/ultraviolet absorption spectrum and the dispersion of the real polarizability in near-resonant regions of pyrimidine, the near-edge absorption fine structure (NEXAFS) of ammonia, and the direct determination of the C_6 dipole−dipole dispersion coefficient of the benzene dimer.

1. INTRODUCTION

Within the field of molecular physics, *electronic response theory* has come to denote formulations of time-dependent perturbation theory as applied to approximate-state electronic structure theory. Today we benefit from 40 years of development work that has led to a situation where linear and nonlinear response functions have been formulated and implemented for the great majority of standard electronic structure methods.[1,2] For example, the linear response function, which is of concern in the present work, has been derived and implemented at the levels of Hartree−Fock,[3−9] Kohn−Sham density functional theory,[6,10−21] second-order polarization propagator approach,[22,23] multiconfiguration self-consistent field,[3−5] second-order Møller−Plesset,[24,25] second-order algebraic-diagrammatic construction,[26,27] and coupled-cluster theory.[28−33]

Among those listed, coupled-cluster (CC) response theory stands out as the most accurate alternative with a fast and systematic convergence of electron correlation with respect to electron excitations in the cluster operator. Truncations made in the cluster operator to include the complete manifolds up to single, double, and triple excitations define a hierarchy of approximations denoted as CCS (coupled-cluster singles), CCSD (coupled-cluster singles and doubles), and CCSDT (coupled-cluster singles, doubles, and triples), respectively, and with certain additional approximations in the manifolds of double and triple excitations, the CC2 (coupled-cluster singles and approximate doubles)[34] and CC3 (coupled-cluster singles, doubles, and approximate triples)[32] members are obtained, which have reduced computational scalings as compared to CCSD and CCSDT, respectively. It has been demonstrated that, by means of the resolution of identity approximation, CC2 response calculations with use of more than 1000 basis functions become feasible,[35,36] moving the target of applications from benchmarking work to applied sciences.

The key feature that makes response theory such a powerful tool in computational spectroscopy is its generality, providing a framework that encompasses a large number of spectroscopies that are seemingly different in nature. In many cases, a mere change of operators in the response functions alters the application from one spectroscopy to another. For example, two electric-dipole operators in the linear response function is the relevant alternative in addressing a refractive index measurement, whereas a mix of one electric-dipole and one magnetic-dipole operator is the relevant choice in addressing an optical rotatory dispersion measurement. In addition, one can pursue a residue analysis of response functions and determine transition energies and the corresponding moments, so that it becomes possible to address spectroscopies based on photon absorption although the response functions themselves are divergent in regions of resonances in the spectrum. In standard response theory, such absorption properties are obtained from solutions to the generalized eigenvalue problem, usually found in a bottom-up fashion by means of iterative algorithms. Typically only the first few valence excited states are identified in such schemes, which is prohibitive when addressing (large) systems with a high density of states or when one is concerned with high-energy photons. In the X-ray region, for example, there are a vast number of excitation energies below and around the core excitations of interest. A pragmatic way to address high-lying excitations can be to construct a limited Hessian based on a restricted set of electron excitation operators, but the important relaxation mechanism for the frozen orbitals is then disregarded.

As an alternative to a residue analysis for addressing resonance spectroscopies, the inclusion of finite excited-state lifetimes has been considered for response calculations in different contexts.[5,37−46] Reflecting different physical aspects, a selection of names can be given to the resulting response formulation, e.g., complex polarization propagator (CPP) theory, resonant convergent response theory, or damped response theory. We will use CPP as an abbreviation throughout this work, and note

Received: December 22, 2011
Published: March 14, 2012

that the CPP approach overcomes the difficulties mentioned above by the introduction of relaxation (damping) mechanisms in the equations of motion, leading to response functions that are resonance convergent and which correspond to physical observables also in regions of electronic resonances. Rather than the excited states being solved to determine transition properties, the CPP response function itself will be directly proportional to the absorption strength or dichroism.[39−41] In the present paper, we will combine the CPP formulation of a resonance convergent response theory with the coupled-cluster technique to describe the electronic structure. We will consider the hierarchy of CC methods, including CCS, CC2, and CCSD, and in addition, we will adopt the noniterative CCSDR(3) (coupled-cluster singles and doubles with noniterative-triples-corrected excitation energies) model[47] to correct the CCSD transition energies for triple excitations.

Our implementation is based on an asymmetric Lanczos-chain-driven subspace algorithm in which a reduced-space tridiagonal representation of the asymmetric CC Jacobian is constructed, enabling calculations of the CPP-CC response function for an arbitrary frequency interval and given damping term. Diagonalization of the tridiagonal representation of the Jacobian yields the individual excitation energies, and from the reduced-space left and right eigenvectors the complex response function is constructed. Moreover, these eigenvectors can be used to determine the eigenvectors of the full-space Jacobian and the oscillator strengths of the individual transitions and to analyze the nature of the transitions. The use of the iterative asymmetric Lanczos algorithm to determine damped linear response functions follows closely developments within vibrational CC response theory.[44−46]

We will illustrate a selection of the novel opportunities for simulations of spectroscopic properties that open up with the development of complex coupled-cluster response theory, in comparison with conventional linear response CC theory. First, we will determine the ultraviolet/visible (UV/vis) absorption spectrum of pyrimidine to investigate what chain length is needed in the Lanczos algorithm to fully reproduce the corresponding absorption spectrum determined by means of conventional response theory. Second, we will present the real part of the electric-dipole polarizability of pyrimidine in the UV/vis region and show how the divergencies of conventional response theory affect near-resonant results. Third, we will determine the near-edge X-ray absorption fine structure (NEXAFS) spectrum of ammonia. We will also in this example illustrate the convergence behavior with respect to the chain length and see how it differs between X-ray and UV/vis spectroscopies. In addition, we will investigate how the quality of the X-ray absorption spectrum depends on the adopted manifold of electron excitation operators. It is to be anticipated that inclusion of double excitations is imperative since it provides a first contribution to the relaxation of the valence electron density in the vicinity of the core hole. Fourth, we will demonstrate how the CPP-CC approach provides a means to compute the polarizability with an imaginary frequency argument and thus allow for a determination of dispersion interaction energies. We will obtain the C_6 coefficient of benzene at the CCSD level of theory and compare our results against experimental results of benchmarking quality. However, before the presentation of numerical results, we will, in the next section, provide the theory and details of our implementation.

2. THEORY

2.1. Exact Standard and Damped Linear Response Function. In exact theory, the linear response function $\langle\langle X;Y\rangle\rangle_\omega$ for two generic operators, X and Y, is given by

$$\langle\langle X;\, Y\rangle\rangle_\omega = -\sum_j \left(\frac{\langle 0|X|j\rangle\langle j|Y|0\rangle}{\omega_j - \omega} + \frac{\langle 0|Y|j\rangle\langle j|X|0\rangle}{\omega_j^* + \omega} \right) \tag{1}$$

This response function is seen to diverge when the frequency ω of the external field approaches any one of the transition frequencies ω_j of the system. As discussed in, e.g., refs 5, 37, and 43, one can introduce damping terms in the linear response function that represent the finite lifetimes of the respective excited states and correspond to line broadenings in absorption spectra, thereby yielding the *damped* linear response function

$$\langle\langle X;\, Y\rangle\rangle_\omega^{\{\gamma_j\}} = -\sum_j \left(\frac{\langle 0|X|j\rangle\langle j|Y|0\rangle}{(\omega_j - i\gamma_j) - \omega} + \frac{\langle 0|Y|j\rangle\langle j|X|0\rangle}{(\omega_j - i\gamma_j)^* + \omega} \right) \tag{2}$$

By further adopting a common damping parameter, $\gamma_j = \gamma$, for all excited states, we can write

$$\langle\langle X;\, Y\rangle\rangle_\omega^{\gamma} = -\sum_j \left(\frac{\langle 0|X|j\rangle\langle j|Y|0\rangle}{\omega_j - (\omega + i\gamma)} + \frac{\langle 0|Y|j\rangle\langle j|X|0\rangle}{\omega_j + (\omega + i\gamma)} \right) \tag{3}$$

where the imaginary $i\gamma$ term is now conveniently associated with the external frequency ω, rather than the excitation energy ω_j. Thus, damped linear response theory effectively corresponds to introducing a complex optical frequency, $\omega \rightarrow \omega + i\gamma$, which implies solving response equations with complex frequencies.[5,7,37,43] Note that the effective broadening introduced by the empirical damping parameter γ in reality has a number of physical origins, including spontaneous-emission broadening, Doppler broadening, vibrational broadening, and collisional broadening. Many of these different physical effects are in essence outside the pure electronic space considered here. In addition, they do not all generally give rise to Lorentzian line shape functions as obtained by the above form. However, in realistic terms, detailed knowledge of all these different effects is hard if not impossible to achieve. In this regard, the introduction of the damping/broadening parameter γ is attractive from a pragmatic as well as a theoretical point of view, as it seeks to model effects that are not included in the undamped response functions. As a side benefit, this also gives the response functions more regular behavior when considered as a function of frequency (finite values at resonant frequencies) and when considered as a matrix function of the relevant response matrix (vide infra).

2.2. Coupled-Cluster Standard and Damped Linear Response Function. In standard coupled-cluster response theory, the linear response function $\langle\langle X;Y\rangle\rangle_\omega$ is computed according to[33]

$$\langle\langle X;\, Y\rangle\rangle_\omega = \frac{1}{2} C^{\pm\omega} \{ \eta_\mu^X t_\mu^Y(\omega) + \eta_\mu^Y t_\mu^X(-\omega) + F_{\mu\nu} t_\mu^X(-\omega) t_\nu^Y(\omega) \} \tag{4}$$

in terms of the coupled-cluster "building blocks"[33]

$$\xi_\mu^X = \langle \mu | \exp(-T) X \exp T | \mathrm{HF} \rangle \tag{5}$$

$$\eta_\mu^X = \langle \Lambda | [X, \tau_\mu] \exp T | \mathrm{HF} \rangle \tag{6}$$

$$A_{\mu\nu} = \langle \mu | \exp(-T) [H, \tau_\nu] \exp T | \mathrm{HF} \rangle \tag{7}$$

$$F_{\mu\nu} = \langle \Lambda | [[H, \tau_\mu], \tau_\nu] \exp T | \mathrm{HF} \rangle \tag{8}$$

where T is the cluster operator, $T = \sum_\mu t_\mu \tau_\mu$, with t_μ indicating the cluster amplitude and τ_μ the excitation operator, and $\langle \Lambda | = \langle \mathrm{HF} | + \sum_\lambda \bar{t}_\lambda \langle \lambda | e^{-T}$. Summation over repeated indices is implied here and throughout. $C^{\pm\omega}$ is the symmetrization operator, $C^{\pm\omega} f(\omega) = \{f(\omega) + f^*(-\omega)\}$. The response amplitudes $\mathbf{t}^Y(\omega)$ are obtained by solving the response equations

$$(\mathbf{A} - \omega \mathbf{1}) \mathbf{t}^Y(\omega) = -\boldsymbol{\xi}^Y \tag{9}$$

where $\mathbf{A}$ is the coupled-cluster Jacobian matrix of eq 7.

In analogy with the exact case, the damped equivalents of the CC linear response function, eq 4, and response equation, eq 9, are obtained by replacing the frequency ω by the complex frequency $\omega + i\gamma$

$$\langle\langle X; Y \rangle\rangle_\omega^\gamma = C^{\pm(\omega)} \{ \eta_\mu^X t_\mu^Y(\omega + i\gamma) + \eta_\mu^Y t_\mu^X(-\omega - i\gamma) + F_{\mu\nu} t_\mu^X(-\omega - i\gamma) t_\nu^Y(\omega + i\gamma) \} \tag{10}$$

which requires the solution of complex linear response equations such as

$$(\mathbf{A} - (\omega + i\gamma)\mathbf{1}) \mathbf{t}^Y(\omega + i\gamma) = -\boldsymbol{\xi}^Y \tag{11}$$

See ref 46 for an argument of why this form gives the exact damped response function in the limit of a complete cluster expansion.

In the following, we will illustrate how one can compute the complex response function by means of an asymmetric Lanczos-chain method. Since the focus in this paper is only on isotropic properties such as energies and isotropic polarizabilities, we will, in the next sections, limit ourselves to the case where the operators are identical, i.e., $X = Y$.

2.3. Asymmetric Lanczos Method. The Lanczos algorithm is a well-known iterative method to transform a general (large) matrix to a (smaller) tridiagonal form more easily diagonalized or inverted.[48] The Lanczos algorithm is of particular importance when information on the whole spectrum is desired.[49] In our context, the matrix to be tridiagonalized is the asymmetric Jacobian matrix $\mathbf{A}$ (of dimensions $n \times n$) of the previous section, and its tridiagonal asymmetric transform is $\mathbf{T}$

$$\mathbf{T} = \mathbf{P}^\mathrm{T} \mathbf{A} \mathbf{Q} \qquad \mathbf{P}^\mathrm{T} \mathbf{A} = \mathbf{T} \mathbf{P}^\mathrm{T} \qquad \mathbf{A} \mathbf{Q} = \mathbf{Q} \mathbf{T} \tag{12}$$

where

$$\mathbf{P}^\mathrm{T} \mathbf{Q} = \mathbf{1} \tag{13}$$

The $\mathbf{Q}$ and $\mathbf{P}^\mathrm{T}$ matrices are formed by, respectively, column ($\mathbf{q}_i$) and row ($\mathbf{p}_i^\mathrm{T}$) vectors known as Lanczos-chain vectors or Lanczos vectors. $\mathbf{T}$ has the form

$$\mathbf{T} = \begin{pmatrix} \alpha_1 & \gamma_1 & 0 & \dots & 0 \\ \beta_1 & \alpha_2 & \gamma_2 & 0 & \vdots \\ 0 & \beta_2 & \alpha_3 & \ddots & 0 \\ \vdots & 0 & \ddots & \ddots & \gamma_{n-1} \\ 0 & \dots & 0 & \beta_{n-1} & \alpha_n \end{pmatrix} \tag{14}$$

The values of the nonzero elements are obtained from the recursive relations

$$\mathbf{A}\mathbf{q}_i = \gamma_{i-1}\mathbf{q}_{i-1} + \alpha_i \mathbf{q}_i + \beta_i \mathbf{q}_{i+1} \tag{15}$$

$$\mathbf{p}_i^\mathrm{T} \mathbf{A} = \beta_{i-1}\mathbf{p}_{i-1}^\mathrm{T} + \alpha_i \mathbf{p}_i^\mathrm{T} + \gamma_i \mathbf{p}_{i+1}^\mathrm{T} \tag{16}$$

for all $i = 1, \dots, n-1$, having assumed $\gamma_0 \mathbf{q}_1 = 0$ and $\beta_0 \mathbf{p}_1^\mathrm{T} = \mathbf{0}$. At iteration $i + 1$, the new $\mathbf{q}_{i+1}$ and $\mathbf{p}_{i+1}^\mathrm{T}$ vectors are generated as

$$\mathbf{q}_{i+1} = \beta_i^{-1}(\mathbf{A}\mathbf{q}_i - \gamma_{i-1}\mathbf{q}_{i-1} - \alpha_i \mathbf{q}_i) = \frac{\mathbf{r}_i}{\beta_i} \tag{17}$$

$$\mathbf{p}_{i+1}^\mathrm{T} = \gamma_i^{-1}(\mathbf{p}_i^\mathrm{T}\mathbf{A} - \beta_{i-1}\mathbf{p}_{i-1}^\mathrm{T} - \alpha_i \mathbf{p}_i^\mathrm{T}) = \frac{\mathbf{s}_i^\mathrm{T}}{\gamma_i} \tag{18}$$

where α_i is straightforwardly computed from the biorthogonality condition given in eq 13:

$$\alpha_i = \mathbf{p}_i^\mathrm{T} \mathbf{A} \mathbf{q}_i \tag{19}$$

Since $1 = \mathbf{p}_i^\mathrm{T}\mathbf{q}_i$, the γ_i and β_i elements are related through $\gamma_i \beta_i = \mathbf{s}_i^\mathrm{T}\mathbf{r}_i$ and any choice of their values satisfying this relation is admissible. Several recipes have been proposed.[42,48] Here we choose $\beta_i = |\mathbf{s}_i^\mathrm{T}\mathbf{r}_i|^{1/2}$, which implies $\gamma_i = (\mathbf{s}_i^\mathrm{T}\mathbf{r}_i)\beta_i^{-1} = \mathrm{sign}(\mathbf{s}_i^\mathrm{T}\mathbf{r}_i)\beta_i$. Also the starting vectors $\mathbf{q}_1$ and $\mathbf{p}_1^\mathrm{T}$ can be chosen freely as long as they satisfy the biorthogonality condition, and we will return to this choice later on. Notice that, to avoid numerical instabilities and the occurrence of spurious poles, in particular for long chain lengths, it is convenient to enforce the biorthogonality condition ($\mathbf{p}_i^\mathrm{T}\mathbf{q}_k = \delta_{ik}$) between the Lanczos vectors at each iteration in the implementation of the Lanczos algorithm.

Truncating the dimension of $\mathbf{T}$ to a certain value k of the *chain length*—which defines the so-called Krylov subspace—we obtain an approximate $\mathbf{T}^{(k)}$ matrix and, from it, generate an approximate representation of the Jacobian matrix $\mathbf{A}$ and of the resolvent matrix $\mathbf{A}(\omega) = \mathbf{A} - \omega\mathbf{1}$. To this end, we define

$$\mathbf{T}^{(k)}(\omega) = \mathbf{T}^{(k)} - \omega \mathbf{1}^{(k)} \tag{20}$$

where $\mathbf{1}^{(k)}$ is an identity matrix of dimension k, and also write

$$\mathbf{A}\mathbf{Q}^{(k)} = \mathbf{Q}^{(k)}\mathbf{T}^{(k)} + \beta_k \mathbf{q}_{k+1} \mathbf{e}_k^{(k)\mathrm{T}} \tag{21}$$

where $\mathbf{Q}^{(k)}$ is the rectangular matrix of dimensions $n \times k$ containing the first k chain vectors $\mathbf{q}_i$. The last term in eq 21 accounts for the truncation error introduced by limiting the dimension of $\mathbf{T}$ to a certain value k of the chain length, expressed using $\mathbf{e}_l^{(k)\mathrm{T}}$ as a row vector of dimension k with element l equal to 1 and all other elements equal to zero. In the following, the truncation error will be neglected, and we can then write

$$\mathbf{A}(\omega)\mathbf{Q}^{(k)} \approx \mathbf{Q}^{(k)}\mathbf{T}^{(k)}(\omega) \tag{22}$$

$$\mathbf{A}^{-1}(\omega)\mathbf{Q}^{(k)} \approx \mathbf{Q}^{(k)}(\mathbf{T}^{(k)}(\omega))^{-1} \tag{23}$$

As seen in eq 4, the computation of the linear response function $\langle\langle X;X\rangle\rangle_{\omega}^{\gamma}$ involves a first contribution of the form

$$(\boldsymbol{\eta}^{X})^{\mathrm{T}}\mathbf{A}^{-1}(\omega)\boldsymbol{\xi}^{X} \equiv n_{\eta}n_{\xi}(\bar{\boldsymbol{\eta}}^{X})^{\mathrm{T}}\mathbf{A}^{-1}(\omega)\bar{\boldsymbol{\xi}}^{X} \tag{24}$$

where n_{η} and n_{ξ} are normalization factors for the $\boldsymbol{\xi}^{X}$ and $\boldsymbol{\eta}^{X}$ vectors, respectively

$$\boldsymbol{\xi}^{X} = n_{\xi}\bar{\boldsymbol{\xi}}^{X} \tag{25}$$

$$\boldsymbol{\eta}^{X} = n_{\eta}\bar{\boldsymbol{\eta}}^{X} \tag{26}$$

determined such that

$$(\bar{\boldsymbol{\xi}}^{X})^{\mathrm{T}}\bar{\boldsymbol{\xi}}^{X} = 1 \tag{27}$$

$$(\bar{\boldsymbol{\eta}}^{X})^{\mathrm{T}}\bar{\boldsymbol{\xi}}^{X} = 1 \tag{28}$$

The last equation is needed to satisfy eq 13, a consequence of the fact that we want to use $\bar{\boldsymbol{\eta}}^{X}$ and $\bar{\boldsymbol{\xi}}^{X}$ as initial vectors of, respectively, the P and Q chains

$$\mathbf{q}_1 = \bar{\boldsymbol{\xi}}^{X} = \mathbf{Q}^{(k)}\mathbf{e}_1^{(k)} \tag{29}$$

$$\mathbf{p}_1^{\mathrm{T}} = (\bar{\boldsymbol{\eta}}^{X})^{\mathrm{T}} = \mathbf{e}_1^{(k)\mathrm{T}}\mathbf{P}^{(k)\mathrm{T}} \tag{30}$$

This choice of starting vectors proves to be quite convenient as it simplifies the final computational expression of the damped response function, and it is important for ensuring attractive global convergence properties of the algorithm (vide infra). First, it allows us to recast eq 24 in the form

$$\begin{aligned} &n_{\eta}n_{\xi}\mathbf{e}_1^{(k)\mathrm{T}}\mathbf{P}^{(k)\mathrm{T}}\mathbf{A}^{-1}(\omega)\mathbf{Q}^{(k)}\mathbf{e}_1^{(k)} \\ &\quad = n_{\eta}n_{\xi}\mathbf{e}_1^{(k)\mathrm{T}}\mathbf{P}^{(k)\mathrm{T}}\mathbf{Q}^{(k)}(\mathbf{T}^{(k)}(\omega))^{-1}\mathbf{e}_1^{(k)} \\ &\quad = n_{\eta}n_{\xi}\mathbf{e}_1^{(k)\mathrm{T}}(\mathbf{T}^{(k)}(\omega))^{-1}\mathbf{e}_1^{(k)} \end{aligned} \tag{31}$$

Let us now assume we can fully diagonalize $\mathbf{T}^{(k)}$ and obtain the biorthonormal left ($\mathbf{L}^{(k)}$) and right ($\mathbf{R}^{(k)}$) eigenvectors

$$\mathbf{T}^{(k)}\mathbf{R}^{(k)} = \mathbf{R}^{(k)}\boldsymbol{\Omega}^{(k)} \tag{32}$$

$$\mathbf{L}^{(k)}\mathbf{T}^{(k)} = \boldsymbol{\Omega}^{(k)}\mathbf{L}^{(k)} \tag{33}$$

with $\mathbf{L}^{(k)}\mathbf{R}^{(k)} = \mathbf{1}^{(k)}$ and $\boldsymbol{\Omega}^{(k)}$ indicating the diagonal matrix containing the eigenvalues of $\mathbf{T}^{(k)}$. It can then be proved that

$$(\mathbf{T}^{(k)} - \omega\mathbf{1}^{(k)})^{-1} = \mathbf{R}^{(k)}(\boldsymbol{\Omega}^{(k)} - \omega\mathbf{1}^{(k)})^{-1}\mathbf{L}^{(k)} \tag{34}$$

The latter is plugged into eq 31 to yield

$$\begin{aligned} &n_{\eta}n_{\xi}\mathbf{e}_1^{(k)\mathrm{T}}\mathbf{R}^{(k)}(\boldsymbol{\Omega}^{(k)} - \omega\mathbf{1}^{(k)})^{-1}\mathbf{L}^{(k)}\mathbf{e}_1^{(k)} \\ &\quad = n_{\eta}n_{\xi}\sum_{j}\frac{L_{j1}^{(k)}R_{1j}^{(k)}}{\omega_j - \omega} \end{aligned} \tag{35}$$

The second contribution to the linear response function, the one involving the $\mathbf{F}$ matrix, is also simplified by the above choice of starting vectors, since we have simply approximated the amplitude equation as

$$\begin{aligned} \mathbf{t}^{X}(\omega) &= -n_{\xi}(\mathbf{A} - \omega\mathbf{1})^{-1}\bar{\boldsymbol{\xi}}^{X} \approx -n_{\xi}\mathbf{Q}^{(k)}(\mathbf{T}^{(k)}(\omega))^{-1}\mathbf{P}^{(k)\mathrm{T}}\bar{\boldsymbol{\xi}}^{X} \\ &= -n_{\xi}\mathbf{Q}^{(k)}\mathbf{R}^{(k)}(\boldsymbol{\Omega}^{(k)} - \omega\mathbf{I}^{(k)})^{-1}\mathbf{L}^{(k)}\mathbf{P}^{(k)\mathrm{T}}\bar{\boldsymbol{\xi}}^{X} \\ &= -n_{\xi}\mathbf{Q}^{(k)}\mathbf{R}^{(k)}(\boldsymbol{\Omega}^{(k)} - \omega\mathbf{I}^{(k)})^{-1}\mathbf{L}^{(k)}\mathbf{e}_1^{(k)} \end{aligned} \tag{36}$$

such that

$$\sum_{\mu\nu}F_{\mu\nu}t_{\mu}^{X}(-\omega)\,t_{\nu}^{X}(\omega) \approx {n_{\xi}}^{2}\sum_{jl}\mathcal{F}_{jl}\frac{L_{j1}^{(k)}L_{l1}^{(k)}}{(\omega - \omega_j)(\omega + \omega_l)} \tag{37}$$

with $\mathcal{F}_{jl} = \sum_{\mu\nu}F_{\mu\nu}(\mathbf{Q}^{(k)}\mathbf{R}^{(k)})_{\mu j}(\mathbf{Q}^{(k)}\mathbf{R}^{(k)})_{\nu l}$.

Thus, given the above choices of biorthonormal vectors $\bar{\boldsymbol{\xi}}^{X}$ and $\bar{\boldsymbol{\eta}}^{X}$ as starting vectors of the Lanczos chain and using the eigenvectors and eigenvalues of the $\mathbf{T}^{(k)}$ matrix yields the following simplified diagonal representation of the damped linear response function (isotropic component):

$$\begin{aligned} \langle\langle X;\,X\rangle\rangle_{\omega}^{\gamma} &= n_{\eta}n_{\xi}\sum_{j}\left\{\frac{L_{j1}^{(k)}R_{1j}^{(k)}}{(\omega - \omega_j) + \mathrm{i}\gamma} - \frac{L_{j1}^{(k)}R_{1j}^{(k)}}{(\omega + \omega_j) + \mathrm{i}\gamma}\right\} \\ &\quad - {n_{\xi}}^{2}\sum_{jl}\mathcal{F}_{lj}\frac{L_{j1}^{(k)}L_{l1}^{(k)}}{(\omega - \omega_j + \mathrm{i}\gamma)(\omega + \omega_l + \mathrm{i}\gamma)} \end{aligned} \tag{38}$$

The damped response function can be split into real and imaginary components. Assuming for simplicity that only real eigenvalues are obtained (even though this is not strictly guaranteed due to the non-Hermitian nature of the coupled-cluster Jacobian), the real and imaginary components of the complex response functions can be written as

$$\begin{aligned} &\mathcal{R}\langle\langle X;\,X\rangle\rangle_{\omega}^{\gamma} \\ &\quad = n_{\eta}n_{\xi}\sum_{j}L_{j1}^{(k)}R_{1j}^{(k)}\left\{\frac{\omega - \omega_j}{(\omega - \omega_j)^2 + \gamma^2} - \frac{\omega + \omega_j}{(\omega + \omega_j)^2 + \gamma^2}\right\} \\ &\qquad - {n_{\xi}}^{2}\sum_{jl}\frac{[\mathcal{F}_{jl}L_{j1}^{(k)}L_{l1}^{(k)}](\omega^2 + \gamma^2 - \omega\omega_j + \omega\omega_l - \omega_j\omega_l)}{[(\omega - \omega_j)^2 + \gamma^2][(\omega + \omega_l)^2 + \gamma^2]} \end{aligned} \tag{39}$$

and

$$\begin{aligned} &\mathcal{I}\langle\langle X;\,X\rangle\rangle_{\omega}^{\gamma} \\ &\quad = \gamma n_{\eta}n_{\xi}\sum_{j}L_{j1}^{(k)}R_{1j}^{(k)}\left\{\frac{1}{(\omega - \omega_j)^2 + \gamma^2} - \frac{1}{(\omega + \omega_j)^2 + \gamma^2}\right\} \\ &\qquad - \gamma{n_{\xi}}^{2}\sum_{jl}\frac{\mathcal{F}_{lj}L_{j1}^{(k)}L_{l1}^{(k)}(2\omega + \omega_l - \omega_j)}{[(\omega - \omega_j)^2 + \gamma^2][(\omega + \omega_l)^2 + \gamma^2]} \end{aligned} \tag{40}$$

The implementation also covers the trivial extension to the case where complex roots are encountered.

Having described our Lanczos approach for calculating damped response functions, we emphasize here two aspects of the Lanczos procedure. The first one is the standard view as a diagonalization method. Converging from extreme toward interior eigenvalues, more and more eigenvalues and eigenvectors are converged with increasing chain length. While for a limited

dx.doi.org/10.1021/ct200919e | J. Chem. Theory Comput. 2012, 8, 1616−1628

(say <50) well-separated set of roots such as typically found for smaller closed shell molecules alternative methods such as the Davidson[50] or the Olsen[51] method are likely to be more efficient in terms of the number of **A** transformations needed, this aspect is important, as it provides an open-ended explicit diagonalization method also for dense spectra. The second aspect is that the Lanczos approach provides effective spectra useful for accurate computations of matrix functions. In this regard, we can consider our damped response function as a matrix function of the CC Jacobian matrix. The Lanczos procedure defines an approximation to the true matrix. The matrix functions are accordingly calculated with increasing precision as the chain length increases. As follows in the subsequent subsections, the response function (meaning the matrix function) can be used to describe many different phenomena. We thereby see a concrete Lanczos chain as defined by its length and start guesses as providing a particular simulation of the phenomena under study. The convergence behavior of these matrix equations is related to the convergence of the eigenvalues. However, this matrix perspective also opens for a more global view upon the convergence, and one can prove some concrete attractive results. Specifically, the moments of the spectrum (the nth moment being defined as the integral of the spectrum times the frequency to the nth power) converge with increasing chain length (see refs 45, 46, and 49 for detailed arguments). This can be seen as a remarkable global convergence behavior of the Lanczos method, but at the same time, the lack of a defined absolute convergence error for a given pair of frequency ω and damping γ calls for caution in the calculation.

The Lanczos algorithm has been implemented and works for the CCS, CC2, and CCSD calculations of response functions. The calculation of the CC3 response is presently not feasible in this manner, since the triple-excitations part of CC3 is not explicitly present in the calculation, whereas the Lanczos algorithm, as written here, requires full vectors. For partitioned approaches such as current implementations of CC3[32] and RI-CC2 (RI = resolution of the identity),[35,36] further work is thus required for the algorithm to be applicable.

2.4. Properties of Interest. The resonance convergent polarizability of a molecular system can be expressed in terms of the complex linear response function as

$$\alpha_{\alpha\beta}(\omega) = -\langle\langle \mu_\alpha; \mu_\beta \rangle\rangle_\omega^\gamma \tag{41}$$

with μ_α being a Cartesian component of the electric dipole moment operator. This would in principle require the solution of the complex linear response equation in eq 11 over a grid of input frequencies ω and using a single specific damping term γ. However, by adopting the asymmetric Lanczos-chain algorithm, we obtain the entire frequency range as a function of an (approximate) Jacobian matrix, **A**, thus only requiring the construction (by an iterative procedure) of the tridiagonal matrix $\mathbf{T}^{(k)}$, and its diagonalization, once and for all frequency values of interest.

Separating the real and imaginary parts of the complex polarizability, we write

$$\alpha = \alpha^{\mathcal{R}} + i\alpha^{\mathcal{I}} \tag{42}$$

either for a specific tensor component or for the isotropic average, commonly denoted by $\bar{\alpha}$. From the imaginary part of the polarizability, the linear absorption cross-section $\sigma(\omega)$ for a randomly oriented molecular system is given by

$$\sigma(\omega) = \frac{4\pi}{c}\omega\bar{\alpha}^{\mathcal{I}}(\omega) \tag{43}$$

where c is the speed of light. We here compute the imaginary polarizability from eq 40. The real part of the polarizability, on the other hand, relates to the index of light refraction according to the expression

$$n(\omega) = 1 + 2\pi N\bar{\alpha}^{\mathcal{R}}(\omega) \tag{44}$$

In this case, it is assumed that the molecular sample is in the form of a dilute gas, so that local field effects and intermolecular interactions can be disregarded, with a molecular number density N. We obtain the real polarizability from eq 39.

Another example of a property that can be obtained from the complex polarization propagator is the electric dipole polarizability with an imaginary frequency argument, $\alpha(i\omega)$; this is achieved, in eq 3, by letting the optical frequency be equal to zero and instead varying the damping parameter, which, in effect, amounts to $i\gamma \rightarrow i\omega$. In practice, we use the expression in eq 39 with $\omega = 0$. This molecular property enters into the Casimir–Polder integral formula[52] from which the long-range dispersion interaction energy can be determined for systems A and B: the resulting C_6 coefficient is given by

$$C_6 = \frac{3}{\pi}\int_0^\infty \bar{\alpha}^{\mathrm{A}}(i\omega)\bar{\alpha}^{\mathrm{B}}(i\omega)d\omega \tag{45}$$

Also, in this case, we have assumed an isotropic orientational average of the molecular systems.

Finally, the oscillator strengths f_{0j} of the individual excitations $(0 \rightarrow j)$ contributing to a given band can also be straightforwardly computed. They are found as residues of the complex response function in eq 38, which is equivalent to computing the limit for $\gamma \rightarrow 0$ of eq 40

$$f_{0j}^{\beta\beta} = \frac{2}{3}\omega_j\left\{n_\eta n_\xi L_{j1}^{(k)}R_{1j}^{(k)} - {n_\xi}^2\sum_l \mathcal{F}_{lj}\frac{L_{j1}^{(k)}L_{l1}^{(k)}}{(\omega_j + \omega_l)}\right\} \tag{46}$$

here given for a specific Cartesian component β of the electric dipole moment operator.

2.5. Spectral Assignments and Convergence Monitoring. Even though the imaginary polarizability yields directly the absorption spectrum by virtue of eq 43, one may wish to analyze the character of the excitations that contribute to a given spectral feature. In the Lanczos algorithm, this can be done by generating pseudoeigenvectors in full excitation space, via the transformation of the eigenvectors $\mathbf{R}^{(k)}$ and $\mathbf{L}^{(k)}$ of the approximate tridiagonal matrix $\mathbf{T}^{(k)}$ to full space with the **Q** and **P** matrices, respectively:

$$\mathbf{R} = \mathbf{Q}^{(k)}\mathbf{R}^{(k)} \tag{47}$$

$$\mathbf{L} = \mathbf{L}^{(k)}\mathbf{P}^{(k)T} \tag{48}$$

and imposing that the individual pseudoeigenvectors are biorthonormal. For instance, we in the following use such a procedure to identify the dominant excitation in each $\mathbf{R}_i$ eigenvector and to determine the weight of those originating from excitations out of the inner core orbitals.

With increasing chain length, an increasing amount of pseudoeigenvectors will converge to true accurate eigenvectors, allowing standard CC calculations of transition properties. This is a most useful test, but also useful in other ways, such as making noniterative-triples-excitation corrections using CCSDR(3) possible using those CCSD eigenvectors that can be verified to have converged. Indeed, for the generation of the CCSDR(3) spectrum, we use the pseudoeigenvectors in full excitation space obtained from the converged Lanczos eigenvectors as restart vectors of a standard CCSD and CCSDR(3) calculation. In doing so, the full CCSD residuals are generated and standard convergence thresholds are satisfied for all relevant roots. Recall still that the essence of the whole strategy is that we do not need to converge all roots explicitly to obtain accurate response functions.

Without the need to transform to the full space, rigorous convergence of the relevant roots with chain length k can be monitored using the convergence criterion for the residual norm $\|\mathbf{r}_i\|$ of the Lanczos eigenvector $\mathbf{R}_i^{(k)}$ (refs 48 and 53):

$$\|\mathbf{r}_i\| = \beta_k |R_{ki}^{(k)}| \times \|\mathbf{q}_{k+1}\| \tag{49}$$

where $\beta_k = T_{k,k+1}$ (that is, the k,k+1 element of the $\mathbf{T}$ matrix in full space), $\mathbf{q}_{k+1}$ is the column vector k+1 of the $\mathbf{Q}$ matrix, and $|R_{ki}^{(k)}|$ is the absolute value of the last element of the eigenvector $\mathbf{R}_i^{(k)}$, at the extra cost of the determination of the additional $\mathbf{q}_{k+1}$ Lanczos vector.

As a first rough measure of convergence for the absorption spectrum, one could simply visually compare the spectra obtained by increasing the chain length of regular increments. Clearly the increase in chain length from j to k should be sufficiently large so that the spectra will change if not converged. A more accurate estimate is obtained by computing the following error function:

$$e_{j,k}(\omega_1, \omega_2) = \frac{\int_{\omega_1}^{\omega_2} |\sigma^{(k)}(\omega) - \sigma^{(j)}(\omega)| d\omega}{\int_{\omega_1}^{\omega_2} \sigma^{(k)}(\omega) d\omega} \tag{50}$$

where $[\omega_1,\omega_2]$ is the selected frequency interval where convergence is estimated and $\sigma^{(j)}$ and $\sigma^{(k)}$ are the absorption functions calculated for two different chain lengths, j and k, respectively.

All above-mentioned criteria were used to monitor the convergence of our results, as will be discussed in section 4.

3. COMPUTATIONAL DETAILS

The Lanczos-chain-driven damped coupled-cluster response method has been implemented on a local version of the DALTON program.[54] The same program has also been used for standard CCSD linear response (LR-CCSD) calculations that were pursued for comparative purposes. All electrons were correlated in all calculations.

The chosen molecular structure for pyrimidine, see Figure 1, is taken from ref 55 and corresponds to an optimized structure at the MP2/cc-pVTZ level of theory. For the calculation of the UV/vis absorption spectra, we have chosen the basis set denoted cc-pVDZ+ in ref 55 (which is equal to Dunning's standard aug-cc-pVDZ basis set[56] from which the augmenting diffuse functions of highest angular momentum—d for C and p for H—have been removed) and further incremented it with a set of (3s3p3d) Rydberg functions[57] centered at the center of charge. The performance of this basis is studied in ref 55, and it is shown to provide a precision of better than 0.2 eV for excitation energies of valence states and Rydberg states with $n \leq 4$.

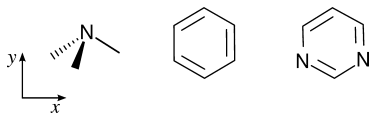

Figure 1. Molecular structures.

The molecular structure for ammonia is taken from experiment,[58] and it corresponds to a bond length of 1.011 Å and a bond angle of 106.7°. For the calculation of the X-ray absorption spectra, we have adopted the standard aug-cc-pCVTZ[59] basis set (which is obtained from the aug-cc-pVTZ set[56] by augmentation with core-polarizing functions[59]) and added a set of (3s3p3d) Rydberg functions centered at the center of charge.

The molecular structure used for benzene is an optimized structure obtained at the density functional theory (DFT) level utilizing the hybrid B3LYP functional[60] and the standard cc-pVTZ basis set.[61] The geometry optimization was carried out with the Gaussian03 program,[62] leading to C−C and C−H bond lengths of 1.391 and 1.082 Å, respectively.

For the calculations of dispersion properties, we have chosen the Sadlej-pVTZ basis set,[63] a basis set which has been optimized with respect to the calculation of static polarizabilities. For the purpose of benchmarking the performance of the Sadlej-pVTZ basis set for calculations of dispersion properties based on CC wave function correlated methods, we have performed property calculations for methane and compared the results obtained using the Sadlej-pVTZ basis set with those obtained using various Dunning x-aug-cc-pVXZ basis sets. In these calculations we have adopted a molecular structure from experiment[64] with a C−H bond length of 1.086 Å.

4. RESULTS AND DISCUSSION

4.1. Ultraviolet/Visible Absorption. As an illustration of the performance of the Lanczos-driven CPP-CC methods for valence excitations, we consider the UV absorption spectrum of pyrimidine, $C_4N_2H_4$, and compare the results obtained using the Lanczos CPP-CCSD algorithm with those from calculations using the standard linear response theory, denoted here LR-CCSD. The spectrum of pyrimidine has been studied extensively in the literature, partly owing to the high degree of symmetry in pyrimidine, which makes it a suitable candidate for demonstrating the performance of novel theoretical models. We direct the reader's attention to a number of experimental,[65−67] theoretical,[68,69] and joint[70−72] studies in addition to the study by Öhrn and Christiansen,[55] to which our present calculations are compared.

Our study is restricted to vertical electronic excitations, and we adopt the spectral assignments made in ref 55. We also refer to this work for a comprehensive comparison between experiments and theoretical results. It is noted that the lowest valence excitations are first n → π^*, followed by $\pi \rightarrow \pi^*$, and thereafter weaker Rydberg excitations, although some valence-Rydberg mixing is expected.

Spectra obtained with use of the CPP-CCSD and LR-CCSD methods and spanning the energy region 4.5−9.0 eV are depicted in Figure 2. For the former approach, the convergence of the Lanczos-chain method is investigated and demonstrated

dx.doi.org/10.1021/ct200919e | J. Chem. Theory Comput. 2012, 8, 1616−1628

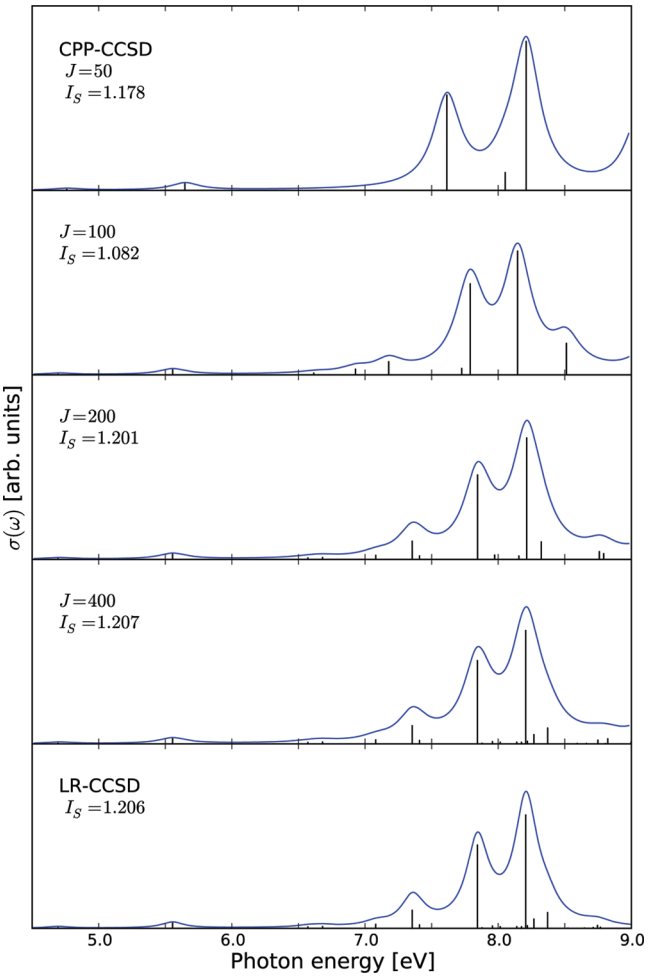

Figure 2. UV absorption spectra for pyrimidine as obtained with CPP-CCSD response theory using the Lanczos algorithm with varying chain length J. Results are compared to the spectrum obtained with conventional LR-CCSD theory using a Lorentzian broadening of 1000 cm^{-1}, as reported in ref 55. The integrated absorption cross-section I_S is reported for the interval up to 8.5 eV.

by comparing spectral differences for calculations employing different values of the chain length J. It can be seen that convergence is reached at a chain length of J = 400, and at this point, the CPP-CCSD spectrum is also equal to the LR-CCSD spectrum, save for a feature in A_1 symmetry at 8.84 eV that is lacking in the LR-CCSD calculations. The reason for the missing feature in the LR-CCSD spectrum is related to the intrinsic limitation of our standard LR-CCSD solver for determining the eigenvalues and eigenvectors of the Jacobian, which is based on a "bottom-up" technique, hereby only allowing us to converge a relatively small number of roots. This limitation could possibly be superseded by alternative windowing and root-following methods.

Apart from this difference, the visual comparison shows excellent agreement between the two approaches. As a more quantitative measure, we report the integrated absorption cross-section I_S of the interval ranging from 0 to 8.5 eV for all spectra and again observe a perfect agreement between the standard LR and CPP approaches. The energy range of this comparison is shortened as compared to the plot interval due to the previously mentioned lack of spectral features in the LR-CCSD results. As the two different methods perform equivalently, we deem the discussion concerning effects of geometry, basis set, CC model, and so on from ref 55 to be transferable to the present study.

In Figure 2, we also demonstrate the convergence of the Lanczos-chain method by visualizing the absorption spectrum as obtained with different chain lengths together with the corresponding values of I_S. It can be seen that the convergence of the method is progressively improved, with more intense roots converging at a lower value of the chain length J. It is also noted that an insufficient value of J can result in spectral features arising from a combination of several states that are not individually resolved in the calculation. Such a "combined" absorption peak appears in the spectrum at an intermediate energy and with an intensity that corresponds to the total absorption intensity of the set of unresolved states. As a consequence, for the integrated absorption cross-section I_S, we do not observe a smooth and monotonic convergence behavior since, for small values of J, combined absorption peaks appear inside or outside the energy region of 0−8.5 eV in a random manner. The results at J = 400 were also compared to those of a reference calculation using J = 800 (for which we obtain the same values of I_S), and an error of 2.1×10^{-5}, as calculated from eq 50, is found.

Should the calculation of the integrated absorption cross-section I_S be done in an exact state theory for the entire frequency range, the Thomas−Reiche−Kuhn sum rule implies that this value should equal the number of electrons in the system. However, in the case of pyrimidine, we obtain a value for the integrated cross-section of only 34.8, as opposed to the exact value of 42. This discrepancy is attributed predominantly to basis set incompleteness, as a reminder that a basis set of mere valence double-ζ quality is employed, and, to a lesser extent, to the use of a nonvariational electronic structure method. We note that the corresponding result for ammonia (vide infra) is 10.1, well in line with the sum rule and reflecting the use of a triple-ζ basis set. However, although the integrated absorption cross-section for pyrimidine is far from converged to the number of electrons in the system, we still note that this property is conserved with respect to differences in chain lengths. This conservation law reflects the tendency of the Lanczos-chain method to combine several adjacent roots to fewer strong roots while retaining the combined oscillator strength.

The importance of including double excitations in the coupled-cluster excitation manifold for a specific transition can be measured by studying the relative norm of these amplitudes in the pseudoexcitation vectors as compared to the norm of all amplitudes. We report double-excitation contributions for excitations with energies below 9.0 eV that range from 4.4% to 9.4%, with a mean value of 5.8%. The most prominent $\pi \rightarrow \pi^*$ features at 7.84 and 8.21 eV have doubles contributions of 6.3% and 6.2%, respectively.

Altogether, the damped CC response function approach to calculating standard UV/vis absorption spectra presents itself as a viable alternative to standard LR-CC procedures. In the present example, there are no significant computational gains. Using a relatively tight convergence in the LR-CC response equations, the Lanczos approach is marginally faster, producing a good absorption spectrum by means of 200 iterations. For small molecules with few and relatively well-separated low-lying states, conventional response calculations provide for several reasons the better alternative. However, for systems with a higher density of states, on the other hand, the balance will shift and the Lanczos approach will be the better alternative. In addition, we note that the Lanczos calculation provides the

spectrum covering the entire energy range. We will return to this point later in a discussion of the X-ray absorption spectrum of ammonia.

4.2. Refractive Index. Considering the dispersion of the complex polarizability for a molecular system as expressed in eq 42, where the frequency ω is implicit, it is possible to simultaneously consider both attenuation and frequency-dependent refraction of a propagating light beam. In this section, we address the real part of the polarizability, from which we can determine the refractive index by virtue of eq 44 or the frequency-dependent relative permittivity $\varepsilon_r(\omega) = n^2(\omega)$.

The real part of the polarizability of pyrimidine over a range of frequencies has been determined in the course of the same CPP-CCSD calculations using a chain length of $J = 800$ referred to in the previous section, and the results are shown in Figure 3.

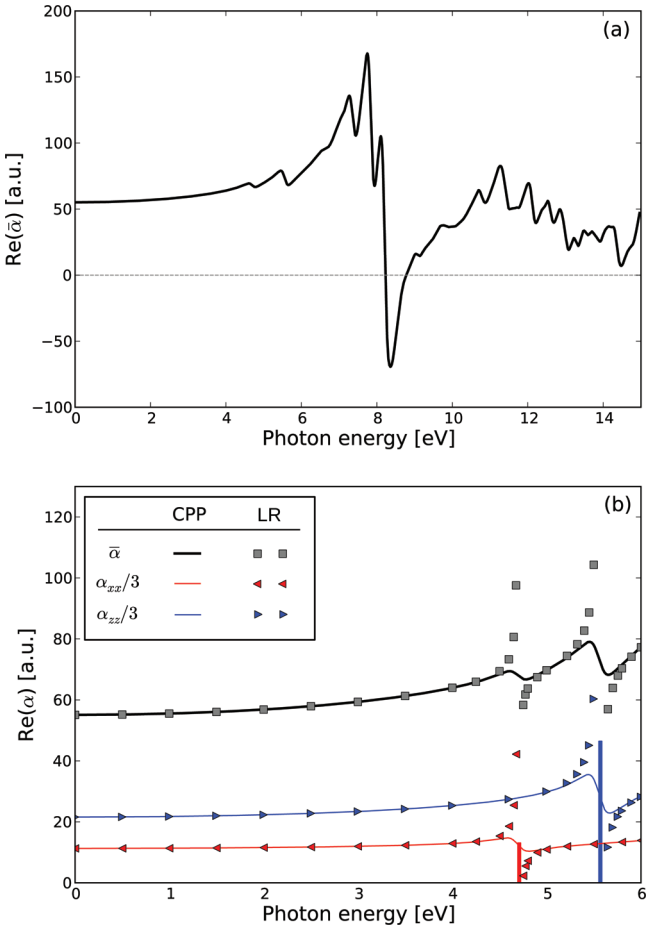

Figure 3. Dispersion of the real part of the polarizability for pyrimidine as obtained at the CCSD level of theory in conjunction with CPP and at the conventional linear response CCSD level of theory: (a) CPP results for the isotropic average and (b) CPP and LR results for the isotropic average as well as two diagonal tensor components. The two lowest singlet excited states are indicated by bars representing oscillator strengths. All results are obtained with a chain length of $J = 800$.

Specifically, in Figure 3a, we illustrate the isotropic average of said polarizability over a frequency interval from 0 to 15 eV and observe negative values at approximately 8.4 eV. This yields a refractive index of less than 1 and corresponds to a situation where the phase velocity of the radiation is greater than the speed of light. This behavior can be difficult to observe experimentally since it occurs at frequencies that are strongly absorptive. At the modest chain length of 50, we report an accuracy of 0.001 au for the static polarizability, indicating that the permittivity for frequencies below that of the first resonance can be reliably obtained at a very low cost (short chain length) within the Lanczos-chain approach.

In Figure 3b we report again the isotropic average of the real part of the polarizability as well as the two tensor components α_{xx} and α_{zz} for which resonances occur in correspondence to excited states of B_1 and B_2 symmetry, respectively. Included in the figure are also results obtained using LR-CCSD at a selection of discrete frequencies, and a shorter energy interval is used for ease of comparison. It can be seen that CPP and LR give equivalent results for energies sufficiently far from resonance, whereas LR-CCSD is unable to yield reliable results close to resonances, where the LR-CCSD response functions are divergent. In contrast, the CPP-CCSD response functions are convergent and well-defined for all frequencies, and in combination with the Lanczos-chain approach, we obtain results for the entire frequency region rather than requiring the construction of a grid of specified frequencies. For clarity, the electronic transitions in the interval along with their relative oscillator strengths are included as bars in the figure and correspond to the n $\rightarrow \pi^*$ transition at 4.70 eV and the $\pi \rightarrow \pi^*$ transition at 5.55 eV. The divergences for the associated components of the LR-CCSD polarizabilities are evident in the figure.

4.3. Near-Edge X-ray Absorption. The CPP-CC method is of particular interest for studies of core excitation processes, where a proper description of relaxation effects is essential. When an electron is removed from the core, the wave function will undergo significant relaxation. In the CPP-CC approach we use one set of orbitals, and in the present case this is the ground-state Hartree−Fock orbitals. This means we use the CC response approach to describe the relaxation and correlation effects together through the flexibility of the wave function ansatz. The performance of the method is demonstrated for the K-edge NEXAFS spectrum of ammonia, where we also address the performance of different chain lengths and a hierarchy of coupled-cluster methods. Experimental[73−75] and theoretical[74−77] studies of this system can be found in the literature. We will adopt the experimental (and computational) work by Schirmer et al.[74] as the main reference for our calculated spectra.

As the Lanczos method shows a more rapid convergence of extremal eigenvalues—that is, from the top and bottom of the full spectrum—it can be anticipated that convergence issues will arise when addressing the absorption at the core ionization edges. As a consequence, a longer chain length will be required to achieve spectral convergence in the NEXAFS region as compared to the UV/vis region, and we illustrate this effect in Figure 4 by calculations at the CCSD level of theory. We observe a progressive convergence of the spectral features, showing that several weaker absorption peaks are combined into stronger ones for calculations employing inadequate chain lengths.

Looking at the 1s $\rightarrow$ 3p(e) transition (second peak) in Figure 4, we also observe that two spectral features associated with two different polarizability components converge slowly to a common transition energy at a chain length of about 1500. Therefore, in calculations adopting inadequate chain lengths, caution is called for not to confuse the two contributions as two separate states in the system.

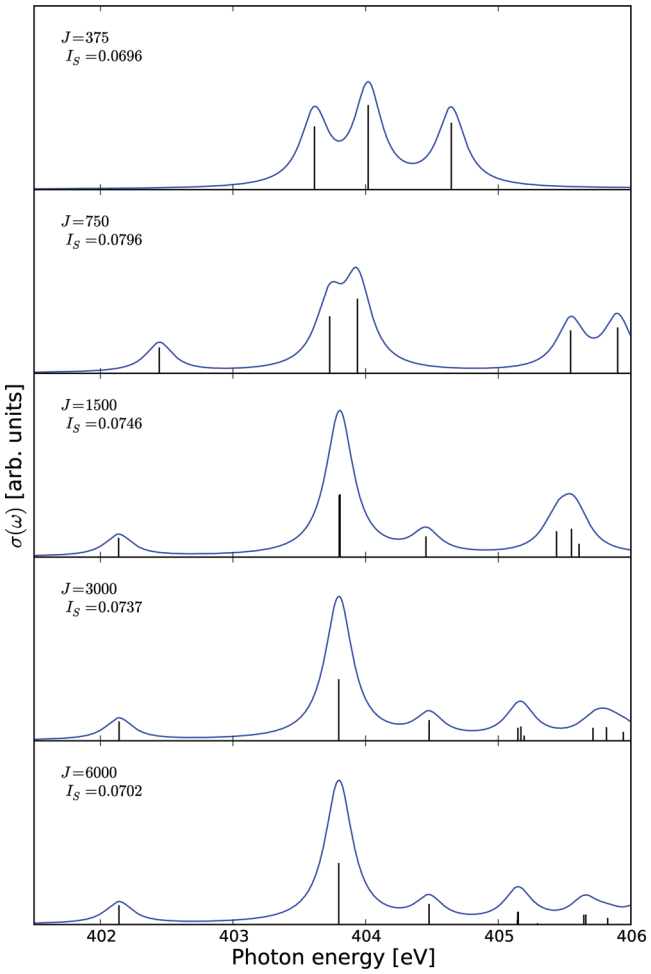

Figure 4. X-ray absorption spectra for ammonia as obtained with CPP-CCSD response theory using the Lanczos algorithm with varying chain length J.

Included in Figure 4 is also the integrated absorption cross-section I_S for the studied energy interval (i.e., 401.5−405.0 eV). A calculation with a chain length of 8000 is also carried out as a reference (yielding $I_S = 0.0706$), and it shows that the spectrum illustrated in the figure for $J = 6000$ is for all practical purposes fully converged; the error is as small as 8.0×10^{-5} using the error function defined in eq 50. Compared to the UV/vis region, where convergence of the absorption spectrum of pyrimidine was achieved for $J = 400$, we note that about 1 order of magnitude longer chain length is needed in the X-ray region.

Using the same error function, the convergence of the Lanczos method is illustrated in Figure 5, which shows the error estimate for varying chain lengths, computed with respect to the reference calculation with chain length $k = 8000$. The variation of the error function is clearly not monotonic over the presented chain length region, not entirely surprising considering the convergence characteristics of the Lanczos method and the fact that we are targeting interior excitations; still its value progressively decreases with increasing chain length.

The coupled-cluster methodology provides a well-defined and systematic way of improving the accuracy by means of an extended excitation manifold. This opens up the possibility of gradually improving the CPP-CC results using the hierarchy of different coupled-cluster methods, and we illustrate this aspect in Figure 6. Included is also the experimental spectrum as

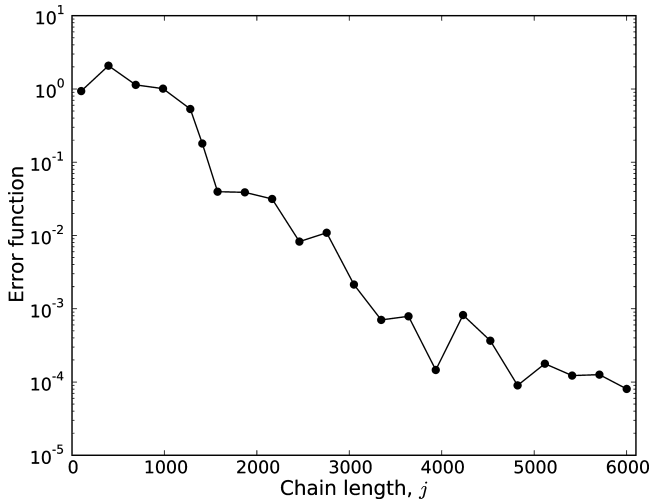

Figure 5. Convergence behavior of the error function $e_{j,k}$ in eq 50 for the X-ray absorption spectrum of ammonia in the frequency interval from 401.5 to 405.0 eV, as obtained from the asymmetric Lanczos algorithm at the CCSD level of theory. The error function for the spectra obtained at various chain lengths j is shown with respect to a reference spectrum computed using a Lanczos chain length k = 8000.

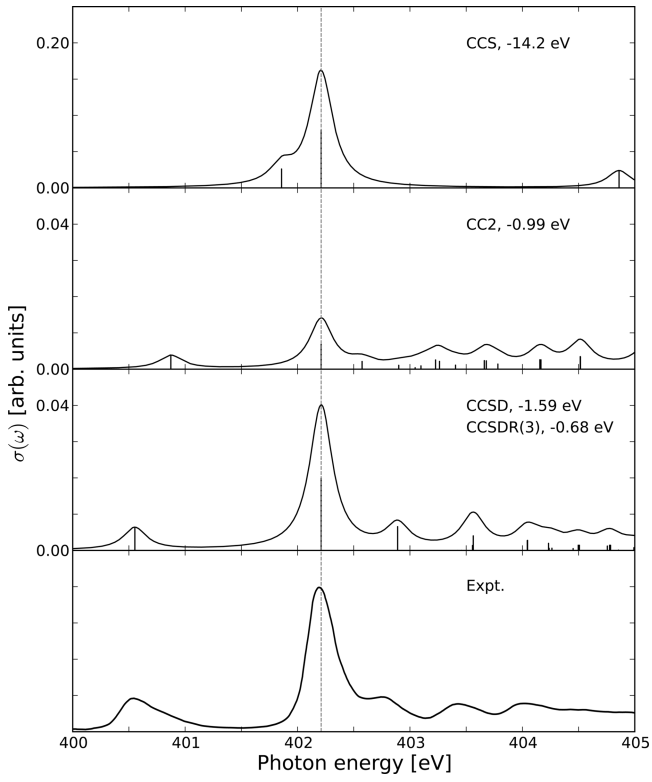

Figure 6. X-ray absorption spectra for ammonia as obtained with damped CC response theory using the hierarchy of CC approximations CCS, CC2, CCSD, and CCSDR(3). CC2 and CCSD spectra are obtained with chain lengths of J = 5000 and 8000, respectively, whereas the full excitation space is spanned for CCS. The experimental spectrum is reprinted from ref 74. Copyright 1993 American Institute of Physics.

obtained from ref 74, and all results are shifted with given energies for an overlap of the 1s → 3p(e) (second peak) transition with experiment. The theoretical results are obtained using CCS, CC2, and CCSD utilizing the chain lengths 426,

dx.doi.org/10.1021/ct200919e | J. Chem. Theory Comput. 2012, 8, 1616−1628

5000, and 8000 for the respective calculations. Note that, for this particular system and basis set, the CCS calculation is fully converged at the adopted chain length; i.e., the tridiagonal matrix **T** is an exact representation of the coupled-cluster Jacobian. The strongly reduced number of roots in the CCS spectrum inflicts largely overestimated oscillator strengths as compared to those for CCSD as a consequence of the fact that the integrated absorption remains more or less conserved. This remark becomes apparent in view of the different scales used for the plotting of the corresponding spectra in Figure 6. It is also clear that the transition energies are largely overestimated in the uncorrelated CCS model, and the applied overall shift of −14.2 eV for the CCS spectrum refers to the missing electronic relaxation/correlation energy.

We also report the energy shift of the CCSD results by means of triple-excitation corrections obtained using CCSDR(3), as acquired for the first two peaks in the CCSD spectrum corresponding to the 1s → 3s(a_1) and 1s → 3p(e) transitions, respectively. The resulting shift accounts for a decrease in excitation energies by 0.91 eV. The energy shifts obtained from the remaining transitions are less reliable due to less converged eigenvectors from the CCSD calculations, and we thus, use the shifts from the aforementioned transitions. We conclude that one needs to reach at least CCSD in the hierarchical set of CC models to obtain accurate X-ray absorption spectra, but even at this point there is a need to apply small overall energy shifts (about 10% of the relaxation/correlation energy is still unaccounted for). With use of the CCS and CC2 models, one obtains incorrect transition energies or intensities or both. The missing relaxation/correlation energy appears smaller in the CC2 model as compared to the CCSD model. However, this is clearly an effect of error cancellation between incomplete treatment of double excitations and neglect of (connected) triple excitations. Note the much improved overall agreement between theoretical and experimental spectra when turning from the CC2 to the CCSD level of theory.

As mentioned before, the importance of including double excitations can be quantified from a study of the elements in the pseudoeigenvectors, specifically by determining the percentage weight of the two-electron excitation component on the total vector (measured as the norm of the double-excitation amplitudes divided by the norm of all amplitudes in the excitation vector times 100). At the CCSD level and for the K-edge of ammonia, this contribution amounts to 11.3−12.1%, which is to be compared with an average contribution of double excitations of 5.8% in the UV/vis absorption spectrum of pyrimidine (see section 4.1). These estimates are expected to be prototypical for systems in general and reflect the stronger requirement on wave function flexibility in the X-ray region to capture the electronic relaxation. Not shown here, we have also determined the UV/vis absorption spectrum for ammonia at the CCSD level of theory, and we then note contributions of double excitations ranging from 4.7% to 4.9% for the first four intense roots in the spectrum.

As the kinetic energies of core electrons are large, strong effects from relativity are to be expected. Ideally, core excitations should be investigated in a fully relativistic framework,[78] and since relativistic and correlation effects are nonadditive, we would, in principle, wish to apply four-component CC methods in the present work. Fortunately, however, the relevant relativistic effects for K-edge transitions are scalar in nature, and as such they can be accounted for by means of the Douglas−Kroll−Hess scalar relativistic Hamiltonian.[79−81] The effects are quite small for such a light element as nitrogen, and we report a positive shift in excitation energies of 0.18−0.19 eV for the peaks in the K-edge spectrum of ammonia.

Additional applications of the CPP-CC method to the calculation of NEXAFS spectra are discussed elsewhere.[82]

4.4. C_6 Dipole−Dipole Dispersion Coefficients. As previously mentioned, by setting the optical frequency to zero (static case) and varying instead the damping term $i\gamma$ in the calculation, it is possible to utilize the present CPP-CCSD method as a means to determine the polarizability at imaginary frequencies. In practice, we employ eq 39. We illustrate this possibility for the cases of methane and benzene and determine the C_6 dipole−dipole dispersion coefficient for the respective dimers, averaged over all molecular orientations. From the C_6 coefficient, the interaction energy in the van der Waals region is given as

$$\Delta E = -\frac{C_6}{R^6} \tag{51}$$

The C_6 coefficient for the dimer is obtained using the Casimir−Polder relation in eq 45, where A = B. This integral can be evaluated using a Gauss−Legendre integration scheme, with a transformation of variables as suggested in ref 83 and followed by a Gauss−Legendre quadrature in the interval $-1 \leq t \leq +1$. The convergence of the scheme is illustrated for benzene in ref 84, where it is shown to be obtained using an eight-point scheme at the time-dependent Hartree−Fock level of theory. In the present work, we use a 12-point scheme for the calculation of the C_6 coefficient.

The isotropic average of the polarizability for imaginary frequencies of benzene can be seen in Figure 7. It displays the expected smooth and monotonic dispersion, as opposed to the dispersion on the real frequency axis, which is strong and oscillatory in the vicinity of electronic transition frequencies; see Figure 3a. The dispersion of $\bar{\alpha}(i\omega)$ is for this reason often described by means of the London approximation according to

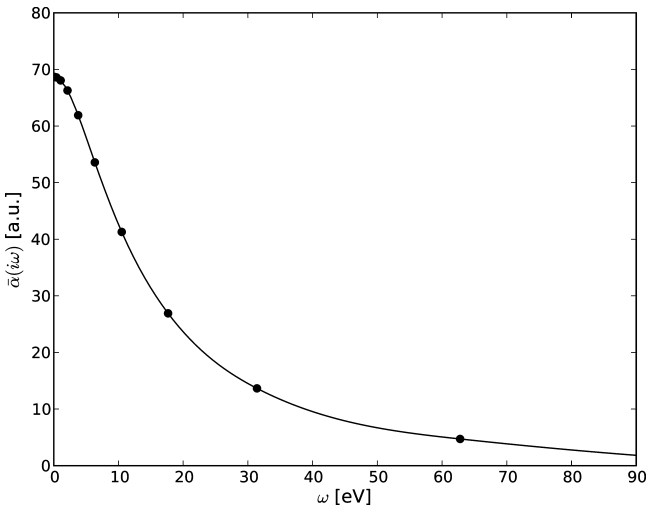

Figure 7. Isotropic average of the polarizability $\bar{\alpha}(i\omega)$ of benzene as a function of the imaginary frequency.

$$\bar{\alpha}(i\omega) = \frac{\bar{\alpha}(0)}{1 + (\omega/\omega_1)^2} \tag{52}$$

where ω_1 is known as a characteristic frequency.

With the aim to obtain an accurate theoretical estimate, we briefly assess the performance of the Sadlej-pVTZ basis against a hierarchy of Dunning's correlation-consistent *x*-aug-cc-pV*X*Z basis sets (with augmentation *x* from single to triple and cardinal number *X* = D, T) for both the static polarizibility and the C_6 dispersion coefficient. Inspecting the results for methane in Table 1, we note a discrepancy of less than half a percent

Table 1. Static Polarizabilities and Dipole−Dipole Dispersion Coefficients for Methane and Benzene[a]

method	ref	α_{xx}	α_{yy}	α_{zz}	$\bar{\alpha}$	C_6
		Methane[b]				
TDHF/d-aug-cc-pVDZ	85	16.16	16.16	16.16	16.16	118.5
TDDFT/d-aug-cc-pVDZ	85	17.20	17.20	17.20	17.20	127.1
CCSD/aug-cc-pVDZ	this work	16.38	16.38	16.38	16.38	121.3
CCSD/d-aug-cc-pVDZ	this work	16.49	16.49	16.49	16.49	121.8
CCSD/d-aug-cc-pVTZ	this work	16.41	16.41	16.41	16.41	121.1
CCSD/t-aug-cc-pVTZ	this work	16.41	16.41	16.41	16.41	121.1
CCSD/Sadlej	this work	16.46	16.46	16.46	16.46	120.8
DOSD	87				17.27	129.6
		Benzene[b]				
TDHF/Sadlej	84	79.69	79.69	45.31	68.23	1737
TDDFT/Sadlej	84	82.74	82.74	44.58	70.02	1773
CCSD/Sadlej	84	81.4	81.4	43.0	68.6	
CCSD/Sadlej+6	86	80.7	80.7	44.9	68.8	
CCSD/Sadlej	93	80.57	80.57	44.66	68.60	
CCSD/Sadlej	this work	80.7	80.7	44.7	68.7	1779
CCSD/d-aug-cc-pVTZ	93	80.35	80.35	44.49	68.40	
CCSD/aug-cc-pVQZ	93	80.14	80.14	44.25	68.18	
CCSD/aug-cc-pVDZ	93	80.09	80.09	44.83	68.34	
CC3/aug-cc-pVDZ	93	79.24	79.24	44.59	67.69	
DOSD	88				67.79	1723

[a]CPP-CCSD results obtained using a chain length of 5000 and 1000 for methane and benzene, respectively. All quantities are expressed in atomic units. [b]Using eq 52, the ZPVA corrections to the static isotropic polarizability $\Delta\bar{\alpha}^{\mathrm{ZPVA}}$ have been determined at the Hartree−Fock/Sadlej-pVTZ level of theory in the B3LYP/cc-pVTZ force field, amounting to 0.96 and 2.12 au for methane and benzene, respectively.

when comparing the Sadlej-pVTZ basis set and the most extensive Dunning correlation-consistent basis sets. It is thus concluded that the Sadlej-pVTZ basis set is a good choice for the calculation of dispersion properties at the electron-correlated CCSD level of theory, in addition to being computationally tractable for a system as large as benzene.

In Table 1, we include experimental values and results from previous theoretical studies at the time-dependent Hartree−Fock (TDHF)[84,85] level, the time-dependent density functional theory (TDDFT) level with the hybrid B3LYP exchange-correlation functional,[84,85] and the CCSD level of theory.[84−86] We compare with experiment in terms of dipole oscillator strength distribution (DOSD) results,[87,88] which are based on a broad compilation of optical and X-ray experimental data. The DOSD result therefore includes the zero-point vibrational averaged electronic contribution but excludes the pure-vibrational contribution, which also has not been calculated in the present work. Including first-order anharmonicity in the potential and polarizability, the perturbation theory expression for the zero-point vibrational average (ZPVA) correction reads[89]

$$\Delta\bar{\alpha}^{\mathrm{ZPVA}} = [\bar{\alpha}]^{0,1} + [\bar{\alpha}]^{1,0} \tag{53}$$

$$[\bar{\alpha}]^{0,1} = -\frac{1}{4}\sum_a \left(\sum_b F_{abb}/\omega_b\right)\frac{\partial\bar{\alpha}}{\partial Q_a}/\omega_a{}^2 \tag{54}$$

$$[\bar{\alpha}]^{1,0} = \frac{1}{4}\sum_a \frac{\partial^2\bar{\alpha}}{\partial Q_a{}^2}/\omega_a \tag{55}$$

where Q_a and ω_a denote the mass-weighted coordinate and vibrational frequency of normal mode *a*, respectively, and *F* is the cubic force field. The superscripts on the respective contribution indicate the degree of electrical (former index) and mechanical (latter index) anharmonicity. For computational ease, the factor $^1/_4\sum_b F_{abb}/\omega_b$ has been identified as the derivative of the zero-point vibrational energy.

A previous study at the TDDFT level of theory[84] for methane is referenced among the tabulated data and seemingly gives more accurate results than the present CPP-CCSD method, if we only regard electronic effects. However, for a correct comparison to be made, the ZPVA correction should be included. For the static polarizability, this correction has been found to amount to 0.90 au at both the Hartree−Fock[90] and MP2[91] levels of theory and using vibrational perturbation theory as well as at the Hartree−Fock and CAM-B3LYP levels of theory with explicit anharmonic wave functions.[92] Using eq 52, we have determined the ZPVA correction to be 0.96 au at the Hartree−Fock/Sadlej-pVTZ level of theory in conjunction with the B3LYP/cc-pVTZ force field. This ZPVA correction shifts the results of the present work closer to experiment, in fact now overshooting the DOSD slightly, with remaining effects anticipated to be due to primarily triple-excitation effects. Applying a 5.5% ZPVA correction to the polarizability in the Casimir−Polder expression implies a corresponding 11% increase in the C_6 coefficient, thereby correcting the pure electronic result of 120.8 au to become equal to 134 au. This result is to be compared with the DOSD result of 129.6 au, indicating that a small negative contribution is to be expected from triples excitations.

For benzene, we first observe that the present CCSD results for static polarizabilities are in close agreement with previous CCSD calculations.[84,86,93] In comparison with uncorrelated results, it is seen that the CCSD results are about 0.7 au larger than previous TDHF results for the in-plane components and 0.6 au smaller for the out-of-plane component. Theoretical results for the C_6 coefficient have been presented in the study by Jiemchooroj et al.[84] at the TDHF and TDDFT levels of theory, and they amount to 1737 and 1773 au, respectively. DFT and CC agree on a 2% positive correlation correction to C_6, but the nature of this correlation correction is different. In the DFT calculation, there is a relatively large correction to the static polarizability which is countered by a stronger dispersion [i.e., larger value of the effective frequency in eq 52], whereas, in the CCSD calculation, the correction to the static polarizability is more modest (about 0.5 au).

The zero-point vibrational average correction has been determined also for benzene using Hartree−Fock/Sadlej-pVTZ property results in combination with the B3LYP/cc-pVTZ force field. At this level of theory, we obtain a ZPVA correction to the static isotropic polarizability that amounts to 2.12 au, leading to an estimate for the total value of $\bar{\alpha}(0)$ equal to 70.8 au.

This theoretical value overshoots the DOSD result of 67.79 au by 4%. Inclusion of triple-excitation effects lowers the static polarizability, as demonstrated in the extensive study of Hammond, Kowalski, and deJong,[93] who obtained a reduction of about −0.65 au from CCSD and CC3, depending somewhat on the basis set. This lowering only makes up for a very small fraction of the difference between our results and DOSD for the static isotropic polarizability. Our pure electronic value for the C_6 coefficient amounts to 1779 au, and with a predicted ZPVA increase of around 6% and a 1% lowering due to triples, our best estimate for this property becomes around 1867 au as compared to the DOSD result of 1723 au.[88]

Given these circumstances in combination with the reputed quality and stability of the CCSD (and CC3) approximation, we have some concerns about the accuracy of the experimental DOSD result for benzene,[88] but more elaborate calculations are required to clarify these details completely.

5. CONCLUSIONS

The resonance convergent linear response function has been implemented on the basis of an asymmetric Lanczos−chain algorithm for the sequence of coupled-cluster response methods CCS, CC2, and CCSD and with corrections to the excited-state energetics due to triple excitations approximately accounted for by means of the noniterative CCSDR(3) approximation. The resonance convergent linear response function allows computation of absorption spectra over the entire frequency range and second-order molecular properties close to resonances as well as at imaginary frequency values. Prototypical examples include the UV/vis absorption spectrum of pyrimidine, the attenuation and frequency-dependent refraction index of the same molecule in near-resonant regions, the NEXAFS of ammonia, and the direct determination of the C_6 coefficient of the benzene dimer.

For standard polarizability calculations the Lanczos procedure converges fast, at a cost only slightly higher than that for the standard methodology for a single frequency, but giving simultaneously the possibility to evaluate the polarizability for a range of (complex) frequencies. The concrete approximation of a complete dispersion curve is a significant attractive feature compared to standard linear response theory. An alternative in this regard is the use of Cauchy moments defined from derivatives of the standard linear response function with respect to frequency.[94] The Cauchy moments require additional equations to be solved, and use of Padé approximants is recommended to obtain lower and upper bounds for C_6; see, e.g., refs 94 and 95.

In the X-ray region, where conventional eigensolver methodologies based on a bottom-up strategy would fail because of the high density of excited states, the Lanczos procedure proves to be a valuable possibility, even though relatively large values of chain length are required.

AUTHOR INFORMATION

Corresponding Author

*E-mail: coriani@units.it.

Notes

The authors declare no competing financial interest.

ACKNOWLEDGMENTS

S.C. acknowledges financial support from the FP7-PEOPLE-2009-IEF funding scheme (Project 254326). P.N. acknowledges financial support from the Swedish Research Council (Grant 621-2010-5014) and a grant for computing time at the National Supercomputer Centre (NSC), Sweden.

REFERENCES

(1) Norman, P. *Phys. Chem. Chem. Phys.* **2011**, *13*, 20519−20535.
(2) Helgaker, T.; Coriani, S.; Jørgensen, P.; Kristensen, K.; Olsen, J.; Ruud, K. *Chem. Rev.* **2012**, *112*, 543−631.
(3) Olsen, J.; Jørgensen, P. *J. Chem. Phys.* **1985**, *82*, 3235−3264.
(4) Jørgensen, P.; Jensen, H. J. Aa.; Olsen, J. *J. Chem. Phys.* **1988**, *89*, 3654−3661.
(5) Norman, P.; Bishop, D. M.; Jensen, H. J. Aa.; Oddershede, J. *J. Chem. Phys.* **2001**, *115*, 10323−10334.
(6) Coriani, S.; Høst, S.; Jansik, B.; Thogersen, L.; Olsen, J.; Jørgensen, P.; Reine, S.; Pawlowski, F.; Helgaker, T.; Salek, P. *J. Chem. Phys.* **2007**, *126*, 154108.
(7) Kauczor, J.; Jørgensen, P.; Norman, P. *J. Chem. Theory Comput.* **2011**, *7*, 1610−1630.
(8) Saue, T.; Jensen, H. J. Aa. *J. Chem. Phys.* **2003**, *118*, 522−536.
(9) Villaume, S.; Saue, T.; Norman, P. *J. Chem. Phys.* **2010**, *133*, 064105.
(10) van Gisbergen, S. J. A.; Snijders, J. G.; Baerends, E. J. *J. Chem. Phys.* **1995**, *103*, 9347−9354.
(11) Jamorski, C.; Casida, M. E.; Salahub, D. R. *J. Chem. Phys.* **1996**, *104*, 5134−5147.
(12) Bauernschmitt, R.; Ahlrichs, R. *Chem. Phys. Lett.* **1996**, *256*, 454−464.
(13) Stratmann, R. E.; Scuseria, G. E.; Frisch, M. J. *J. Chem. Phys.* **1998**, *109*, 8218−8224.
(14) Tozer, D. J.; Handy, N. C. *J. Chem. Phys.* **1998**, *109*, 10180−10189.
(15) Görling, A. *Int. J. Quantum Chem.* **1998**, *69*, 265−277.
(16) Hirata, S.; Head-Gordon, M. *Chem. Phys. Lett.* **1999**, *302*, 375−382.
(17) Helgaker, T.; Wilson, P. J.; Amos, R. D. *J. Chem. Phys.* **2000**, *113*, 2983−2989.
(18) Gao, J.; Liu, W.; Song, B.; Liu, C. *J. Chem. Phys.* **2004**, *121*, 6658−6666.
(19) Gao, J.; Zou, W.; Liu, W.; Xiao, Y.; Peng, D.; Song, B.; Liu, C. *J. Chem. Phys.* **2005**, *123*, 054102.
(20) Salek, P.; Helgaker, T.; Saue, T. *Chem. Phys.* **2005**, *311*, 187−201.
(21) Bast, R.; Jensen, H. J. Aa.; Saue, T. *Int. J. Quantum Chem.* **2009**, *109*, 2091−2112.
(22) Packer, M. J.; Dalskov, E. K.; Enevoldsen, T.; Jensen, H. J. Aa.; Oddershede, J. *J. Chem. Phys.* **1996**, *105*, 5886−5990.
(23) Bak, K. L.; Koch, H.; Oddershede, J.; Christiansen, O.; Sauer, S. P. A. *J. Chem. Phys.* **2000**, *112*, 4173−4185.
(24) Rice, J. E.; Handy, N. C. *J. Chem. Phys.* **1991**, *94*, 4959−4971.
(25) Aiga, F.; Sasagane, K.; Itoh, R. *J. Chem. Phys.* **1993**, *99*, 3779.
(26) Schirmer, J.; Trofimov, A. B. *J. Chem. Phys.* **2004**, *120*, 11449−11464.
(27) Trofimov, A. B.; Krivdina, I. L.; Weller, J.; Schirmer, J. *Chem. Phys.* **2006**, *329*, 1−10.
(28) Monkhorst, H. *Int. J. Quantum Chem.* **1977**, 421−432.
(29) Dalgaard, E.; Monkhorst, H. J. *Phys. Rev. A* **1983**, *28*, 1217.
(30) Sekino, H.; Bartlett, R. J. *Int. J. Quantum Chem.* **1984**, *26*, 255−265.
(31) Koch, H.; Jørgensen, P. *J. Chem. Phys.* **1990**, *93*, 3333.
(32) Christiansen, O.; Koch, H.; Jørgensen, P. *J. Chem. Phys.* **1995**, *103*, 7429.
(33) Christiansen, O.; Jørgensen, P.; Hättig, C. *Int. J. Quantum Chem.* **1998**, *68*, 1−52.
(34) Christiansen, O.; Koch, H.; Jørgensen, P. *Chem. Phys. Lett.* **1995**, *243*, 409−418.
(35) Hättig, C.; Weigend, F. *J. Chem. Phys.* **2000**, *113*, 5154−5161.
(36) Hättig, C.; Hald, K. *Phys. Chem. Chem. Phys.* **2002**, *4*, 2111−2118.
(37) Norman, P.; Bishop, D. M.; Jensen, H. J. Aa.; Oddershede, J. *J. Chem. Phys.* **2005**, *123*, 194103.

(38) Jensen, L.; Autschbach, J.; Schatz, G. C. *J. Chem. Phys.* **2005**, *122*, 224115.
(39) Ekström, U.; Norman, P. *Phys. Rev. A* **2006**, *74*, 042722.
(40) Jiemchooroj, A.; Norman, P. *J. Chem. Phys.* **2007**, *126*, 134102.
(41) Jiemchooroj, A.; Ekström, U.; Norman, P. *J. Chem. Phys.* **2007**, *127*, 165104.
(42) Rocca, D.; Gebauer, R.; Saad, Y.; Baroni, S. *J. Chem. Phys.* **2008**, *128*, 154105.
(43) Kristensen, K.; Kauczor, J.; Kjærgaard, T.; Jørgensen, P. *J. Chem. Phys.* **2009**, *131*, 044112.
(44) Hansen, M. B.; Seidler, P.; Gyorffy, W.; Christiansen, O. *J. Chem. Phys.* **2010**, *133*, 114102.
(45) Seidler, P.; Hansen, M. B.; Gyorffy, W.; Toffoli, D.; Christiansen, O. *J. Chem. Phys.* **2010**, *132*, 164105.
(46) Thomsen, B.; Hansen, M. B.; Seidler, P.; Christiansen, O. *J. Chem. Phys.* **2012**, *136*, 124101.
(47) Christiansen, O.; Koch, H.; Jørgensen, P. *J. Chem. Phys.* **1996**, *105*, 1451.
(48) Golub, G. H.; van Loan, C. F. *Matrix Computations*, 3rd ed.; The Johns Hopkins University Press: Baltimore, MD, 1996.
(49) Meyer, H. D.; Pal, S. *J. Chem. Phys.* **1989**, *91*, 6195−6204.
(50) Davidson, E. *J. Comput. Phys.* **1975**, *17*, 87−94.
(51) Olsen, J.; Jensen, H.; Jørgensen, P. *J. Comput. Phys.* **1988**, *74*, 265−282.
(52) Casimir, H.; Polder, D. *Phys. Rev.* **1948**, *73*, 360.
(53) Parlett, B. N. *The Symmetric Eigenvalue Problem*; Prentice-Hall: Englewoods Cliffs, NJ, 1980.
(54) DALTON, A Molecular Electronic Structure Program, release DALTON2011, 2011; see http://daltonprogram.org.
(55) Öhrn, A.; Christiansen, O. *Phys. Chem. Chem. Phys.* **2001**, *3*, 730.
(56) Kendall, R.; Dunning, T.; Harrison, R. *J. Chem. Phys.* **1992**, *96*, 6796−6806.
(57) Kaufmann, K.; Baumeistert, W.; Jungen, M. *J. Phys. B: At., Mol. Opt. Phys.* **1989**, *22*, 2223−2240.
(58) Duncan, J.; Mills, I. M. *Spectrochim. Acta* **1964**, *20*, 523.
(59) Woon, D.; Dunning, T. *J. Chem. Phys.* **1995**, *103*, 4572−4585.
(60) Becke, A. D. *J. Chem. Phys.* **1993**, *98*, 5648.
(61) Dunning, T. *J. Chem. Phys.* **1989**, *90*, 1007−1023.
(62) Frisch, M. J.; Trucks, G. W.; Schlegel, H. B.; Scuseria, G. E.; Robb, M. A.; Cheeseman, J. R.; Montgomery, J. A.; , Jr., Vreven, T.; Kudin, K. N.; Burant, J. C.; Millam, J. M.; Iyengar, S. S.; Tomasi, J.; Barone, V.; Mennucci, B.; Cossi, M.; Scalmani, G.; Rega, N.; Petersson, G. A.; Nakatsuji, H.; Hada, M.; Ehara, M.; Toyota, K.; Fukuda, R.; Hasegawa, J.; Ishida, M.; Nakajima, T.; Honda, Y.; Kitao, O.; Nakai, H.; Klene, M.; Li, X.; Knox, J. E.; Hratchian, H. P.; Cross, J. B.; Bakken, V.; Adamo, C.; Jaramillo, J.; Gomperts, R.; Stratmann, R. E.; Yazyev, O.; Austin, A. J.; Cammi, R.; Pomelli, C.; Ochterski, J. W.; Ayala, P. Y.; Morokuma, K.; Voth, G. A.; Salvador, P.; Dannenberg, J. J.; Zakrzewski, V. G.; Dapprich, S.; Daniels, A. D.; Strain, M. C.; Farkas, O.; Malick, D. K.; Rabuck, A. D.; Raghavachari, K.; Foresman, J. B.; Ortiz, J. V.; Cui, Q.; Baboul, A. G.; Clifford, S.; Cioslowski, J.; Stefanov, B. B.; Liu, G.; Liashenko, A.; Piskorz, P.; Komaromi, I.; Martin, R. L.; Fox, D. J.; Keith, T.; M. A. Al-Laham, Peng, C. Y.; Nanayakkara, A.; Challacombe, M.; Gill, P. M. W.; Johnson, B.; Chen, W.; Wong, M. W.; Gonzalez, C.; , Pople, J. A. *Gaussian03*, revision E.01; Gaussian, Inc.: Wallingford, CT, 2004.
(63) Sadlej, A. J. *Collect. Czech. Chem. Commun.* **1988**, *53*, 1995−2016.
(64) Gray, D.; Robiette, A. G. *Mol. Phys.* **1979**, *37*, 1901.
(65) Ferreira da Silva, F.; Almeida, D.; Martins, G.; Milosavljević, A. R.; Marinković, B. P.; Hoffmann, S. V.; Mason, J. N.; Nunes, Y.; Garcia, G.; Limão-Vieira, P. *Phys. Chem. Chem. Phys.* **2010**, *12*, 6717−6731.
(66) Callis, P. R. *J. Chem. Phys.* **1981**, *75*, 5640.
(67) Bolovinos, A.; Tsekeris, P.; Philis, J.; Pantos, E.; Andritsopoulos, G. *J. Mol. Spectrosc.* **1984**, *256*, 240−256.
(68) Del Bene, J. E. *J. Chem. Phys.* **1997**, *106*, 6051.
(69) Shojaei, S. R.; Hajgató, B.; Deleuze, M. S. *Chem. Phys. Lett.* **2010**, *498*, 45−51.
(70) Stener, M.; Decleva, P.; Holland, D. M. P.; Shaw, D. *J. Phys. B: At., Mol. Opt. Phys.* **2011**, *44*, 075203.
(71) Fischer, G.; Cai, Z.-L.; Reimers, J. R.; Wormell, P. *J. Phys. Chem. A* **2003**, *107*, 3093−3106.
(72) Palmer, M. H.; Waiker, I. C. *Chem. Phys.* **1990**, *147*, 19−33.
(73) Lindgren, A.; Gisselbrecht, M.; Burmeister, F.; Kivimäki, A.; Sorensen, S. L. *J. Chem. Phys.* **2005**, *122*, 114306.
(74) Schirmer, J.; Trofimov, A. B.; Randall, K.; Feldhaus, J.; Bradshaw, A.; Ma, Y.; Chen, C.; Sette, F. *Phys. Rev. A* **1993**, *47*, 1136−1147.
(75) Jürgensen, A.; Cavell, R. *Chem. Phys.* **2001**, *273*, 77−89.
(76) Chong, D. P. *J. Electron. Spectrosc.* **2005**, *148*, 115.
(77) Niu, A.; Zhang, Y.; Zhang, W.; Li, J. *Phys. Rev. A* **1998**, *57*, 1912.
(78) Ekström, U.; Norman, P.; Carravetta, V. *Phys. Rev. A* **2006**, *73*, 022501.
(79) Douglas, M.; Kroll, N. *Ann. Phys.* **1974**, *82*, 89−155.
(80) Hess, B. A. *Phys. Rev. A* **1986**, *33*, 3742−3748.
(81) Jansen, G.; Hess, B. *Phys. Rev. A* **1989**, *39*, 6016.
(82) Coriani, S.; Christiansen, O.; Fransson, T.; Norman, P. *Phys. Rev. A* **2012**, *85*, 022507.
(83) Amos, R. D.; Handy, N. C.; Knowles, P. J.; Rice, J. E.; Stone, A. J. *J. Phys. Chem.* **1985**, 89.
(84) Jiemchooroj, A.; Norman, P.; Sernelius, B. E. *J. Chem. Phys.* **2005**, *123*, 124312.
(85) Norman, P.; Jiemchooroj, A.; Sernelius, B. E. *J. Phys. Chem.* **2003**, *118*, 9167.
(86) Christiansen, O.; Hättig, C.; Jørgensen, P. *Spectrochim. Acta* **1999**, *55A*, 509−524.
(87) Thomas, G. F.; Meath, W. J. *Mol. Phys.* **1977**, *34*, 113.
(88) Kumar, A.; Meath, W. J. *Mol. Phys.* **1992**, *75*, 311−324.
(89) Bishop, D.; Luis, J.; Kirtman, B. *J. Chem. Phys.* **1998**, *108*, 10013−10017.
(90) Norman, P. Ph.D. Dissertation No. 517, Linköping Studies in Science and Technology, Linköping University, 1998.
(91) Bishop, D. M.; Gu, F. L.; Cybulski, S. M. *J. Chem. Phys.* **1998**, *109*, 8407.
(92) Kongsted, J.; Christiansen, O. *J. Chem. Phys.* **2007**, *127*, 154315.
(93) Hammond, J. R.; Kowalski, K.; deJong, W. A. *J. Chem. Phys.* **2007**, *127*, 144105.
(94) Hättig, C.; Christiansen, O.; Jørgensen, P. *J. Chem. Phys.* **1997**, *107*, 10592−10598.
(95) Langhoff, P. W.; Karplus, M. *J. Chem. Phys.* **1970**, *52*, 1435−1449.